FEBS Letters 587 (2013) 3122–3128

journal homepage: www.FEBSLetters.org

A single amino acid determines the catalytic efficiency of two alkenal double bond reductases produced by the liverwort *Plagiochasma appendiculatum*

Yifeng Wu [a], Yuanheng Cai [b], Yi Sun [a], Ruixue Xu [a], Haina Yu [a], Xiaojuan Han [a], Hongxiang Lou [a], Aixia Cheng [a,*]

[a] Key Laboratory of Chemical Biology of Natural Products, Ministry of Education, School of Pharmaceutical Sciences, Shandong University, Jinan 250012, China
[b] Biosciences Department, Brookhaven National Laboratory, Upton, NY 11973, USA

ARTICLE INFO

Article history:
Received 1 June 2013
Revised 29 July 2013
Accepted 31 July 2013
Available online 13 August 2013

Edited by Miguel De la Rosa

Keywords:
Alkenal double bond reductase;
Hydroxycinnamyl aldehyde;
Molecular modeling;
Site-directed mutagenesis;
Plagiochasma appendiculatum

ABSTRACT

Alkenal double bond reductases (DBRs) catalyze the NADPH-dependent reduction of the α,β-unsaturated double bond of many secondary metabolites. Two alkenal double bond reductase genes *PaDBR1* and *PaDBR2* were isolated from the liverwort species *Plagiochasma appendiculatum*. Recombinant PaDBR2 protein had a higher catalytic activity than PaDBR1 with respect to the reduction of the double bond present in hydroxycinnamyl aldehydes. The residue at position 56 appeared to be responsible for this difference in enzyme activity. The functionality of a C56 to Y56 mutation in PaDBR1 was similar to that of PaDBR2. Further site-directed mutagenesis and structural modeling suggested that the phenol ring stacking between this residue and the substrate was an important determinant of catalytic efficiency.

1. Introduction

The plant phenylpropanoids phenylpropenes, coumarins, lignans and lignin are all derived from the deamination of L-phenylalanine by L-phenylalanine ammonia lyase. Many phenylpropanoids exhibit broad spectrum antimicrobial activity [1,2] and some are known to act as signaling molecules both in the defense response and in the course of development [3]. Dehydrodiconiferyl derivatives are well-known as potential modulators of plant cell division [3]. The phenylpropanoid pathway can also generate many derivatives with extensive medicinal/health protecting properties, such as podophyllotoxin, matairesinol and secoisolariciresinol [4]. Dihydroconiferyl alcohol is a potentially useful anti-inflammatory agent and phlorizin shows considerable promise for treatment of diatetes mellitus [5–7]. Several oxidoreductases are involved in phenylpropanoid metabolism, i.e. secoisolariciresinol dehydrogenase [8–10], phenylcoumaran benzylic ether reductase [11,12], cinnamyl alcohol dehydrogenase [13,14] and alkenal double bond reductase [4,15]. One of these, alkenal double bond reductase, reduces the double bond present in a variety of α,β-unsaturated aldehydes and ketones. Genes encoding several reductases of this type have been isolated. The product of the *Pinus taeda* gene *PtPPDBR* catalyzes the NADPH-dependent reduction of the α,β-unsaturated double bond of phenylpropenal aldehydes [16]. Its *Arabidopsis thaliana* homologue AtDBR1 (*At5g16970*) converts *p*-coumaryl aldehyde and coniferyl aldehyde into their corresponding dihydrophenylpropanols [4]. The tobacco flavin-free double bond reductase NtDBR shows both regional and stereo-specificity against a variety of α,β-unsaturated compounds with different activating group and substitution patterns [15]. The above enzymes all belong to the zinc-independent, medium chain dehydrogenase/reductase (MDR) superfamily, and share a conserved GXXS motif, known to stabilize both the adenine and nicotinamide moieties of NADPH, along with a glycine-rich motif (either AXXGXXG or GXXGXXG), known to participate in the enzyme's binding with the $NAD(P)^+$ or NAD(P)H pyrophosphate [17].

Here we report the isolation from the liverwort species *Plagiochasma appendiculatum* of two genes closely related in sequence to *NtDBR*, *AtDBR1* and *PtPPDBR*. Although their five prime (5′-UTR) and three prime (3′-UTR) untranslated regions share only 26.3% and 22.7% identity, their open reading frame (ORF) sequences differ by just two residues. Their gene products showed distinct substrate preferences and a non-identical catalytic efficiency towards hydroxycinnamyl aldehydes. Site-directed mutagenesis was used to demonstrate that a mutation to one of the

* Corresponding author. Fax: +86 531 88382019.
E-mail address: aixiacheng@sdu.edu.cn (A. Cheng).

0014-5793/$36.00
http://dx.doi.org/10.1016/j.febslet.2013.07.051

two coding region polymorphisms was sufficient to swap functionality, and it was further shown that the phenol ring stacking interaction between the aromatic residue and the bound *p*-coumaryl aldehyde was responsible for the difference in catalytic rates between the two homologs.

2. Materials and methods

2.1. Chemicals and reagents

The synthesis of *p*-coumaryl aldehyde, *p*-coumaryl alcohol, caffeyl aldehyde, caffeyl alcohol, 5-hydroxyconiferyl aldehyde and 5-hydroxyconiferyl alcohol followed a published procedure [14]. Dihydro-*p*-coumaryl aldehyde, dihydrocaffeyl aldehyde, dihydroconiferyl aldehyde, dihydro-5-hydroxyconiferyl aldehyde and dihydrosinapyl aldehyde were all synthesized from their unsaturated form by reduction with hydrogen in the presence of Pd/C. The purity and identity of all the synthesized reagents was validated using ^{1}H NMR. Trans-coumaryl aldehyde, trans-4-hydroxycinnamic acid and 3,4-dihydroxycinnamic acid were purchased from Alfa Aesar (Heysham, UK). All the other reagents and solvents used were purchased from Sigma–Aldrich (St. Louis, USA).

2.2. cDNA cloning, sequence alignment and analysis, and protein modelling

A *P. appendiculatum* thallus cDNA library [18] was searched to identify two DBR-like sequences, designated *PaDBR1* and *PaDBR2* (sequences lodged with GenBank under accession numbers KF051271 and KF051272). Their deduced polypeptide sequences were aligned with those of various plant double bond reductases using DNAMAN software (Version 5.2.2, Lynnon Biosoft, Canada), and a phylogenetic tree based on the neighbor-joining method was constructed with the help of MEGA 4.0 software [19]. Homology models of the two gene products were generated using the Swiss-model server (http://swissmodel.expasy.org), and predicted docking of the ligand and substrate into the active cavity was obtained by applying AutoDock vina [20]. The resulting models were visualized using PyMOL (http://www.pymol.org/citing).

2.3. Recombinant protein expression and purification

The *PaDBR1* and *PaDBR2* ORFs were amplified from the two cDNA clones using, respectively, primer pairs PaDBR1 F/R and PaDBR2 F/R (Suppl. Table 1). Each of the two resulting amplicons was digested with restriction enzymes (Takara, Japan) for ligation into the corresponding cloning site of the pET32a vector (Novagen). After confirmation by sequencing, the constructs were transferred into *Escherichia coli* BL21 (DE3) to allow the heterologous expression of N-terminally His-tagged recombinant PaDBR1 and PaDBR2 proteins. Expression was induced by the addition of 0.5 mM isopropyl β-D-1-thiogalactopyranoside and incubation at 18 °C for 18 h, and the recombinant proteins were purified by passing a cell extract through a Ni–NTA Sefinose His-bind column, according to manufacturer's recommendations (Bio Basic, Canada). The buffer was exchanged by passing the eluate through an Ultrafiltration

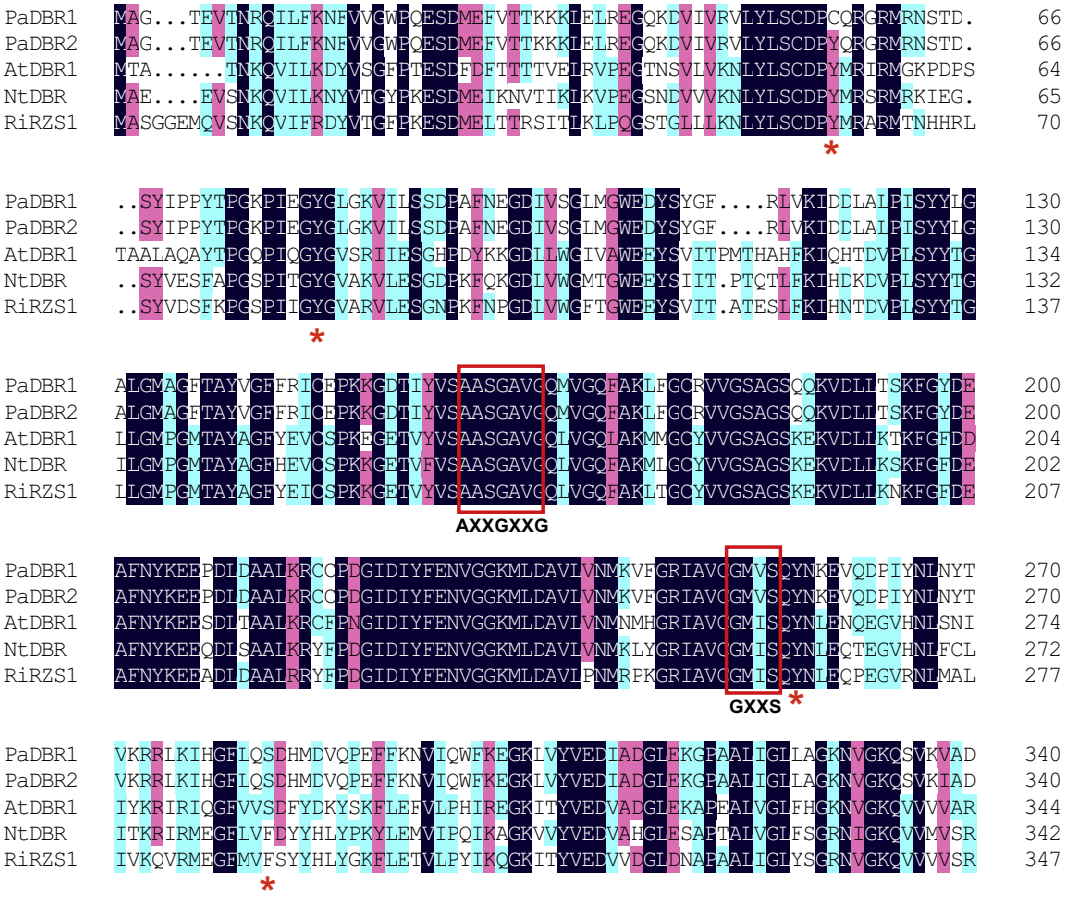

Fig. 1. Peptide alignment of the two PaDBRs with other double bond reductase sequences. AtDBR1 from *A. thaliana* (GenBank accession BT022058), NtDBR from tobacco (BAA89423) and RiRZS1 from raspberry (JN166691). The conserved co-enzyme binding motifs AXXGXXG and GXXS are shown boxed, and active site residues indicated with an asterisk.

tube (Millipore, USA) in the presence of binding buffer (20 mM Tris–HCl, 500 mM NaCl, 5 mM imidazole, pH 8.0). Protein quantification was achieved using the Bradford assay (Bio Rad) with bovine serum albumin used as the standard.

2.4. Enzyme assays

Each 100 μl assay comprised 10 μg purified protein, 400 μM substrate, 1 mM NADPH, made up in 100 mM potassium phosphate buffer, pH 6.0. The reactions were initiated by the addition of the protein and terminated after a 30 min incubation at 37 °C by the addition of 10 μl glacial acetic acid (GAA). The reaction mixture was extracted twice with an equal volume of ethyl acetate, the ethyl acetate fraction evaporated, and the residue dissolved in 100 μl methanol. The methanol solution was subjected to HPLC analysis on a reverse-phase C18 column (XDB-18, 5 μm; Agilent), in which the mobile phase varied linearly over 18 min from 5 parts acetonitrile, 95 parts water containing 3% glacial acetic acid to 25 parts acetonitrile, 75 parts 3% aqueous GAA. The flow rate was 0.8 ml per min and the absorbance of the reaction product was monitored at 280 nm. The enzymatic products were identified by mass spectrometry (MS) using a Shimadzu LCMS-2020 system (Shimadzu Corporation, Japan) with a multi wavelength diode array detector and electron spray ionization mass spectrometer, based on their *m/z* $[M-H]^-$ ion fractions.

The effect on enzymatic activity of altering the solution pH over the range 4–8 was monitored by running the reactions at 35 °C for 30 min in a range of buffers. The optimal temperature was determined in reactions formulated to a pH of 6.0. The enzymes' kinetic parameters were determined by altering substrate concentration (30, 60, 80, 100, 150, 200, 300, 400, 500, 600, 700, 800 μM) in reactions run at the optimal pH and temperature for 10 min. The quantity of reaction product present was estimated from a standard calibration curve.

2.5. Site-directed mutagenesis

Five PaDBR1 mutants were created using Stratagene QuickChange site-directed mutagenesis method. The PaDBR1-pET32a vector served as the template and five pairs of complementary primers were designed using primer X on-line software (http://www.bioinformatics.org/primerx) to generate C56Y, C56F, C56 V, C56A and C56S mutations (Suppl. Table 2). Following the PCR, the wild type PaDBR1-pET32a plasmid was digested by DpnI (Thermo Scientific, USA) at 37 °C for 3.5 h, and a 10 μl aliquot of a gel-purified restriction reaction product was transformed into *E. coli* DH5α. The mutations were first validated by sequencing prior to their heterologous expression in *E. coli* BL21 (DE3). An enzyme assay was performed using both purified PaDBR1 and extracts of the PaDBR1 mutants, using five different hydroxycinnamyl aldehydes as substrate, in reactions set up as described above. Catalytic efficiency was measured by quantifying the amount of reaction product based on a standard calibration curve.

3. Results and discussion

3.1. cDNA isolation and DBR sequence analysis

The length of the *PaDBR1* cDNA clone was 1,371 bp, of which 1026 bp represented the ORF. Its predicted gene product was a

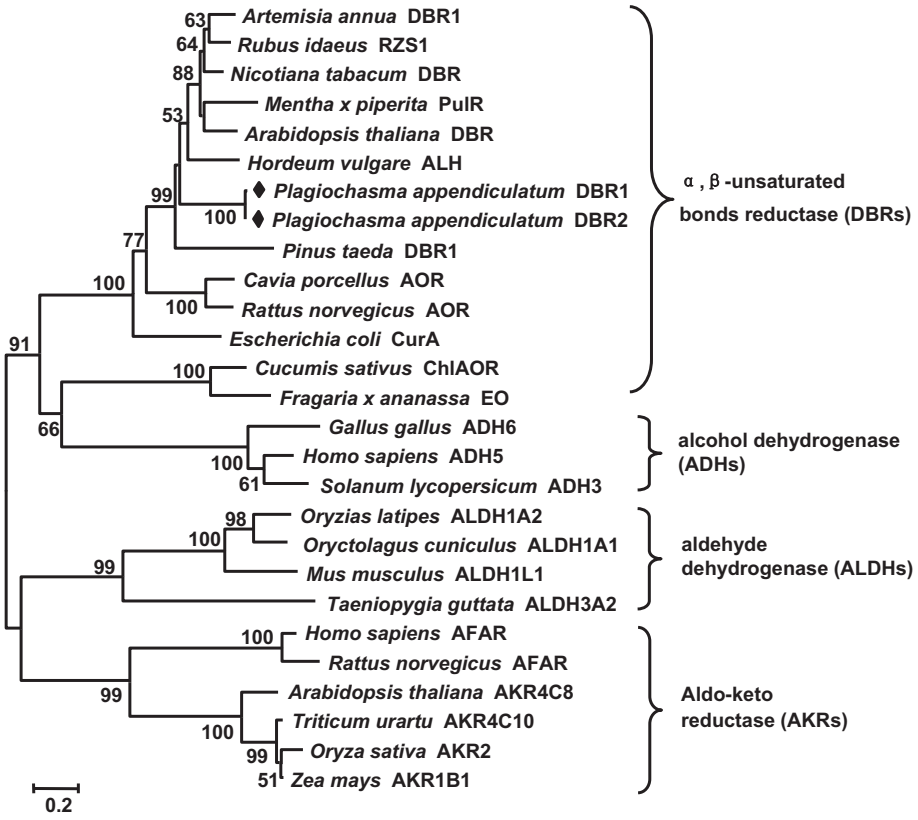

Fig. 2. Phylogenetic relationships among the DBRs, ADHs, ALDHs and AKRs. *Artemisia annua* DBR1 (FJ750460), *Rubus idaeus* RZS1 (JN16669), *Nicotiana tabacum* DBR (BAA89423), *Mentha x piperita* PulR (AY300163), *A. thaliana* DBR (BT022058), *Hordeum vulgare* ALH (AY904340), *Pinus taeda* DBR1 (DQ829775), *Cavia porcellus* AOR (NM_001172980), *Rattus norvegicus* AOR (U66322), *Escherichia coli* CurA (AB583756), *Cucumis sativus* ChlAOR (AB597302), *Fragaria x ananassa* EO (AY048861), *Gallus gallus* ADH6 (NM_205092), *Homo sapiens* ADH5 (NM_000671), *Solanum lycopersicum* ADH3 (NM_001251867), *Oryzias latipes* ALDH1A2 (NM_001104821), *Oryctolagus cuniculus* ALDH1A1 (NM_001082013), *Mus musculus* ALDH1L1 (NM_027406), *Taeniopygia guttata* ALDH3A2 (NM_001245686), *Homo sapiens* AFAR (AF026947), *Rattus norvegicus* AFAR (X74673), *Arabidopsis thaliana* AKR4C8 (DQ837653), *Triticum urartu* AKR4C10 (EMS61074), *Oryza sativa* AKR2 (GQ227709), *Zea mays* AKR1B1 (NP_001105982).

protein consisting of 341 residues with a M_r of 37.8 kDa. The length of the 5′-UTR was 196 bp, and that of the 3′-UTR 149 bp with a 3′ poly (A) tail. The *PaDBR2* cDNA clone was 1,401 bp long, also harboring a 1026 bp ORF which encoded a 341 residue polypeptide of M_r 37.8 kDa. The length of its 5′-UTR was 305 bp, and that of its 3′-UTR 70 bp with a 3′ poly (A) tail. The sequence similarity of the two products at the peptide level was 99.4%: only two residues were polymorphic, namely C56 in PaDBR1 which was represented by Y56 in PaDBR2, and V338 in PaDBR1 (I338 in PaDBR2). The sequences of both UTRs were dissimilar: the sequence identity at the nucleotide level was 26.3% for 5′-UTR and 22.7% for 3′-UTR (Suppl. Fig. 1). Tyrosine at position 56 of PaDBR2 is highly conserved among oxidoreductases, and has therefore been proposed to be involved in binding with NADPH [4]. However, in PaDBR1, this position was occupied by a Cystein residue.

The two PaDBR sequences shared 59.0%, 57.8% and 55.5% identity with, respectively, NtDBR [15], AtDBR1 [4] and RiRZS1 [21] (Fig. 1). Both PaDBRs included the conserved glycine-rich motif AASGAVG, known to participate in the binding of the $NAD(P)^+$ or NAD(P)H pyrophosphate group, as well as a GXXS motif, known to stabilize both the adenine and nicotinamide moieties of NADPH [4]. In order to elucidate the phylogenetic relationships of the PaDBR genes, a phylogenetic tree was constructed using selected α,β-unsaturated bonds reductase (DBR), alcohol dehydrogenase (ADH), aldehyde dehydrogenase (ALDH) and aldo–keto reductase (AKR) sequences from different organisms. The phylogenetic analysis showed that the PaDBRs were included in a clade which contains HvALH, AtDBR1, MpPulR, NtDBR, RiRZS1 and AaDBR1, as well as to the non-plant proteins CpAOR, RnAOR and EcCurA (Fig. 2). The *Rubus idaeus* protein RiRZS1 [21] is responsible for the hydrogenation of the α,β-unsaturated double bond of phenylbutenones in the raspberry fruit. The tobacco enzyme NtDBR [15] shows double bond reductase activity across a number of alternative substrates, while the rat liver enzyme RnAOR [22] catalyzes the reduction of α,β-unsaturated aldehydes and ketones. The phylogeny demonstrated that DBRs, ADHs, ALDHs and AKRs all map to different clades, suggesting a possible evolutionary relationship based on their ability to detoxify reactive carbonyls [23].

3.2. The biochemical and enzymatic properties of the PaDBRs

The molecular weight of each of the two N-terminally His-Tagged recombinant PaDBRs expressed in *E. coli* was about 55 kDa (Suppl. Fig. 2). When PaDBR1 was provided with *p*-coumaryl aldehyde or caffeyl aldehyde as a substrate, the major reaction products exhibited a similar retention time and molecular ion peak as, respectively, *p*-dihydro-*p*-coumaryl aldehyde and dihydrocaffeyl aldehyde (Fig. 3). There was evidence of reactivity when the substrate was either coniferyl or 5-hydroxyconiferyl aldehyde,

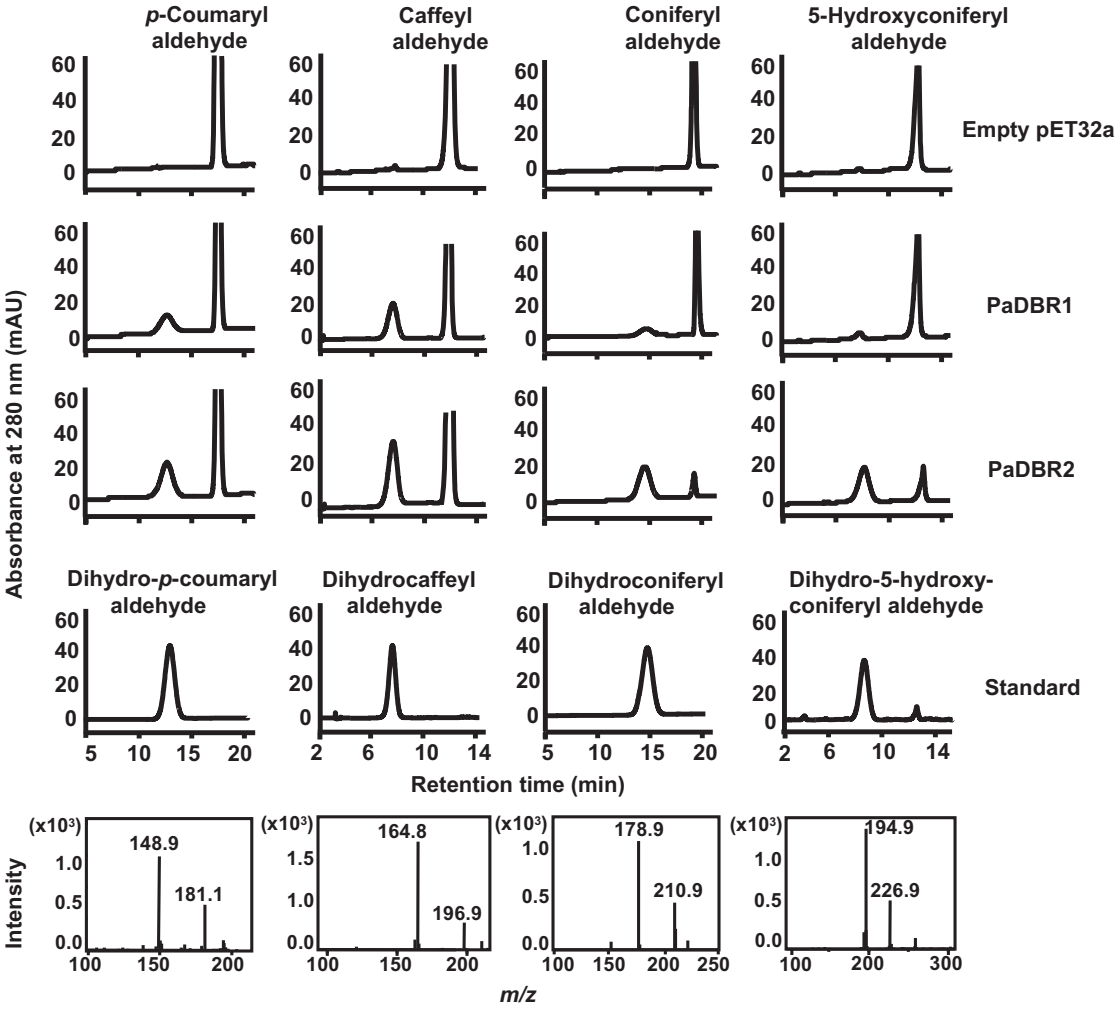

Fig. 3. HPLC profiles and MS spectra of reaction products generated by recombinant PaDBRs. The activities of recombinant PaDBRs when provided with either *p*-coumaryl, cafferyl, coniferyl or 5-hydroxyconiferyl aldehyde as a substrate. The MS spectra of the PaDBR2 reaction products are shown in the lower panel.

but not when it was sinapyl aldehyde. In contrast, PaDBR2 was able to reduce *p*-coumaryl, caffeyl, coniferyl and 5-hydroxyconiferyl aldehyde, and its catalytic efficiency was higher than that of PaDBR1 in each case. PaDBR2 showed trace reactivity with sinapyl aldehyde (data not shown). We suggested the failure to accept sinapyl aldehyde as a substrate of PaDBR1 resulted from that the size of sinapyl aldehyde is larger and sinapyl aldehyde is more hydrophobic than other phenylpropanoid aldehydes. As a result, smaller size and less hydrophobic substrates such as *p*-coumaryl aldehyde or caffeyl aldehyde are the preferred substrates of PaDBR1. The retention time and MS spectra of the major reaction products formed from each substrate are shown in Fig. 3. The optimal temperature for both enzymes was 37 °C and their pH optimum was 6.0. Their K_m, V_{max} and K_{enz} (K_{cat}/K_m) values are given in Table 1. Based on their K_m, the preferred substrate of each enzyme was *p*-coumaryl aldehyde. The graphs for kinetics and pH and temperature were shown in Suppl. Figs. 3 and 4.

Although the two PaDBR sequences differed with respect to two residues, the catalytic efficiency of PaDBR1 was substantially less than that of PaDBR2, especially towards cinnamyl aldehydes carrying a methoxy group (coniferyl, 5-hydroxyconiferyl and sinapyl aldehydes). With respect to AtDBR1, it has been suggested that Y53, Y81, Y260 and S287 (equivalent to C56/Y56, Y81, Y256 and S283 respectively for the PaDBRs) are the key residues determining the enzyme's interaction with NADP$^+$/*p*-coumaryl aldehyde [4]. The sequence alignment implied that the 56C/Y substitution may therefore be responsible for the observed difference in catalytic ability between PaDBR1 and PaDBR2. To test this hypothesis, site-directed mutagenesis was employed to convert 56C to 56Y in PaDBR1. The result of this substitution was that substrate selectivity and catalytic efficiency became indistinguishable from those of PaDBR2 (data not shown). Further mutation of this residue to either F, V, A or S showed that the catalytic efficiency of PaDBR1C56F and PaDBR1C56Y was similar for each substrate tested, and was higher than that of the wild type enzyme – specifically, about three fold higher for *p*-coumaryl, caffeyl aldehydes and ten fold higher for coniferyl and 5-hydroxyconiferyl aldehydes (Table 2). On the other hand, the activities of the PaDBR1C56V, -

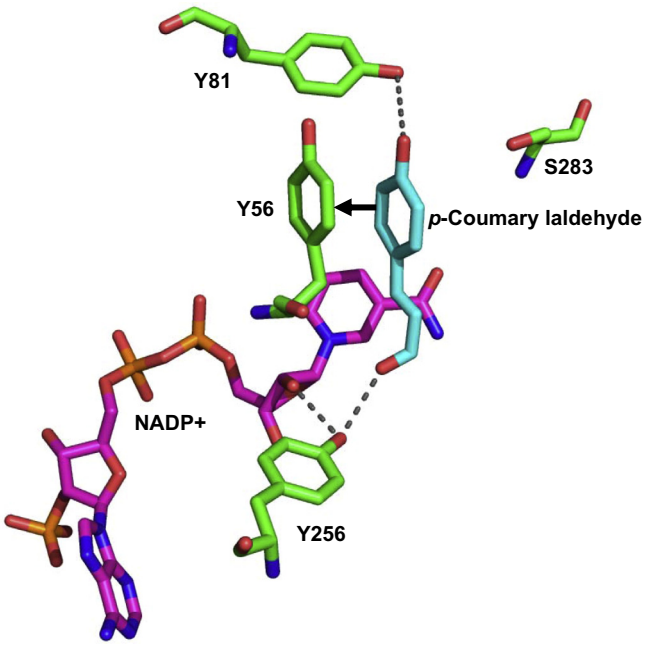

Fig. 4. Docking arrangement of PaDBR1C56Y with NADP+/*p*-coumaryl aldehyde. The arrow indicates a potential stacking interaction between phenol rings. Hydrogen bonds shown as dashed lines.

Table 1
Kinetic parameters of the recombinant PaDBR1, PaDBR2, PaDBR1C56Y and PaDBR1C56V proteins. The substrates are as follows: (1) *p*-Coumaryl aldehyde; (2) Caffeyl aldehyde; (3) Coniferyl aldehyde; (4) 5-Hydroxyconiferyl aldehyde.

Enzyme	Substrate	K_m (μM)	V_{max} (nmol mg^{-1} min^{-1})	K_{cat} (s^{-1})	*K*enz (M^{-1} s^{-1})
PaDBR1	1	171.9 ± 43.0	155.7 ± 14.2	0.098 ± 0.009	570.7
	2	221.4 ± 31.3	210.2 ± 11.1	0.132 ± 0.007	598.2
PaDBR2	1	94.3 ± 22.4	440.4 ± 27.4	0.278 ± 0.017	2949.3
	2	181.2 ± 25.6	377.4 ± 19.4	0.238 ± 0.012	1314.9
	3	209.9 ± 29.4	187.1 ± 11.3	0.118 ± 0.007	562.8
	4	308.1 ± 50.1	267.9 ± 18.3	0.169 ± 0.012	549.0
PaDBR1C56Y	1	118.3 ± 18.9	394.0 ± 22.9	0.249 ± 0.014	2101.9
	2	143.7 ± 23.3	438.2 ± 23.4	0.277 ± 0.015	1924.5
	3	172.6 ± 28.5	212.7 ± 13.0	0.134 ± 0.008	777.7
	4	202.6 ± 27.4	255.2 ± 13.2	0.161 ± 0.008	794.9
PaDBR1C56V	1	166.3 ± 18.0	58.7 ± 2.2	0.037 ± 0.001	222.4
	2	193.3 ± 32.7	107.3 ± 6.7	0.068 ± 0.004	349.7

Table 2
The catalytic efficiency of wild-type PaDBR1 and PaDBR1 mutant proteins. The substrates are as follows: (1) *p*-Coumaryl aldehyde; (2) Caffeyl aldehyde; (3) Coniferyl aldehyde; (4) 5-Hydroxyconiferyl aldehyde; (5) Sinapyl aldehyde; (6) Cinnamyl aldehyde; (7) *p*-Coumaric acid; (8) Caffeic acid; (9) *p*-Coumaryl alcohol; (10) Caffeyl alcohol; (11) Coniferyl alcohol; (12) 5-Hydroxyconiferyl alcohol; (13) Sinapyl alcohol.

	Specific activity (nmol mg^{-1} min^{-1})					
Subtrate	PaDBR1	C56Y mutant	C56F mutant	C56A mutant	C56S mutant	C56V mutant
1	23.70 ± 0.38	74.31 ± 4.64	66.01 ± 1.74	4.09 ± 0.80	7.91 ± 1.04	12.43 ± 2.06
2	17.68 ± 0.61	49.66 ± 1.96	45.42 ± 0.93	7.76 ± 0.31	9.11 ± 0.70	14.95 ± 0.91
3	1.78 ± 0.23	23.85 ± 1.45	27.09 ± 0.36	2.63 ± 0.22	11.54 ± 0.40	8.35 ± 0.49
4	2.66 ± 0.54	23.35 ± 1.23	22.01 ± 2.06	4.64 ± 0.35	11.62 ± 0.23	8.43 ± 0.64
5	ND[a]	Tr[b]	Tr	ND	ND	ND
6–13	ND	ND	ND	–	–	–

[a] No detectable activity.
[b] Trace activity.

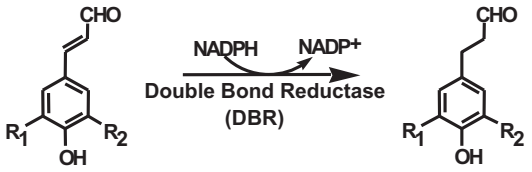

R1,R2= H, *p*-Coumaryl aldehyde
R1=OH; R2=H, Caffeyl aldehyde
R1=OCH3; R2=H, Coniferyl aldehyde
R1=OCH3; R2=OH, 5-Hydroxyconiferyl aldehyde
R1,R2=OCH3, Sinapyl aldehyde

R1,R2=H, Dihydro-*p*-coumaryl aldehyde
R1=OH; R2=H, Dihydrocaffeyl aldehyde
R1=OCH3; R2=H, Dihydroconiferyl aldehyde
R1=OCH3; R2=OH, Dihydro-5-hydroxyconiferyl aldehyde
R1,R2=OCH3, Dihydrosinapyl aldehyde

Fig. 5. Substrates catalyzable by PaDBRs and their corresponding reaction products.

C56S and -C56A enzymes were less effective than those in which an aromatic amino acid was present at position 56. The Y53 residue is conserved across the oxidoreductases and is located between a relatively well conserved short loop and a single turn α helix; its phenol ring in AtDBR1 forms a hydrophobic stacking interaction with the phenol ring of the bound *p*-coumaryl aldehyde, thereby facilitating the orientation of the substrate within the specificity pocket [4]. To verify whether Y56 has a similar role in PaDBRs, the protein structures of PaDBR1 and PaDBR1C56Y were modeled, based on AtDBR1's crystal structure [4]. The model suggested that, just as in AtDBR1, Y56 formed a stacking interaction with the phenol ring of the bound *p*-coumaryl aldehyde (Fig. 4). The Y81 phenolic hydroxyl group was located within a single hydrogen bond distance of the *p*-coumaryl aldehyde's phenolic hydroxyl group. The Y256 phenolic hydroxyl group also was located within hydrogen bonding distance of the *p*-coumaryl aldehyde carbonyl group and the nicotinamide ribose 2'-hydroxyl group. The assumption therefore was that Y256 established hydrogen bonding with both. The hydroxyl groups in Y81 and S283 may also facilitate substrate binding. The suggestion is that the PaDBRs and AtDBR1 share the same catalytic mechanism, while the hydrophobic interaction between Y56 and the substrate's phenolic ring may be a universal feature of plant double bond reductases.

In summary, the PaDBRs were able to reduce hydroxycinnamyl aldehydes (Fig. 5). While several other possible substrates (including cinnamyl aldehyde, hydroxycinnamic acids and alcohols) were tested using PaDBR1 and PaDBR2 (Table 2), none of these compounds was converted into its corresponding dihydro form. The lack of reactivity towards cinnamyl aldehyde indicated the importance of the phenolic hydroxyl group in the hydroxycinnamyl aldehydes. Both PaDBR1 and PaDBR2 lacked any hydrogenation activity when exposed to two diterpenoids, which were purified from an extract of the liverwort species *Jungermannia fauriana* (data not shown),, indicating that the substrate versatility of the PaDBRs is quite low, being mainly involved in the formation of dihydrophenylpropanoid derivatives.

Conflict of interest

The authors declare no conflict of interest in the present investigation.

Acknowledgments

We are grateful for the support of the National Natural Science Foundation of China (No. 31170280), Young Scientists Foundation Grant of Shandong Province (No. BS2010SW019).

Appendix A. Supplementary data

Supplementary data associated with this article can be found, in the online version, at http://dx.doi.org/10.1016/j.febslet.2013.07.051.

References

[1] Dixon, R.A., Achnine, L., Kota, P., Liu, C.J., Reddy, M. and Wang, L. (2002) The phenylpropanoid pathway and plant defence-a genomics perspective. Mol. Plant Pathol. 3, 371–390.
[2] VanEtten, H.D., Mansfield, J.W., Bailey, J.A. and Farmer, E.E. (1994) Two classes of plant antibiotics: phytoalexins versus" phytoanticipins". Plant Cell 6, 1191–1192.
[3] Teutonico, R.A., Dudley, M.W., Orr, J.D., Lynn, D.G. and Binns, A.N. (1991) Activity and accumulation of cell division-promoting phenolics in tobacco tissue cultures. Plant Physiol. 97, 288–297.
[4] Youn, B., Kim, S.J., Moinuddin, S.G., Lee, C., Bedgar, D.L., Harper, A.R., Davin, L.B., Lewis, N.G. and Kang, C. (2006) Mechanistic and structural studies of apoform, binary, and ternary complexes of the Arabidopsis alkenal double bond reductase At5g16970. J. Biol. Chem. 281, 40076–40088.
[5] Karonen, M., Hamalainen, M., Nieminen, R., Klika, K.D., Loponen, J., Ovcharenko, V.V., Moilanen, E. and Pihlaja, K. (2004) Phenolic extractives from the bark of*Pinus sylvestris* L. and their effects on inflammatory mediators nitric oxide and prostaglandin E2. J. Agric. Food Chem. 52, 7532–7540.
[6] Thompson, L.U., Seidl, M.M., Rickard, S.E., Orcheson, L.J. and Fong, H.H. (1996) Antitumorigenic effect of a mammalian lignan precursor from flaxseed. Nutr. Cancer 26, 159–165.
[7] Ehrenkranz, J.R., Lewis, N.G., Kahn, C.R. and Roth, J. (2005) Phlorizin: a review. Diabetes-Metab. Res. Rev. 21, 31–38.
[8] Xia, Z.Q., Costa, M.A., Pelissier, H.C., Davin, L.B. and Lewis, N.G. (2001) Secoisolariciresinol dehydrogenase purification, cloning, and functional expression: implications for human health protection. J. Biol. Chem. 276, 12614–12623.
[9] Youn, B., Moinuddin, S.G., Davin, L.B., Lewis, N.G. and Kang, C. (2005) Crystal structures of apo-form and binary/ternary complexes of Podophyllum secoisolariciresinol dehydrogenase, an enzyme involved in formation of health-protecting and plant defense lignans. J. Biol. Chem. 280, 12917–12926.
[10] Moinuddin, S.G., Youn, B., Bedgar, D.L., Costa, M.A., Helms, G.L., Kang, C., Davin, L.B. and Lewis, N.G. (2006) Secoisolariciresinol dehydrogenase: mode of catalysis and stereospecificity of hydride transfer in*Podophyllum peltatum*. Org. Biomol. Chem. 4, 808–816.
[11] Min, T., Kasahara, H., Bedgar, D.L., Youn, B., Lawrence, P.K., Gang, D.R., Halls, S.C., Park, H., Hilsenbeck, J.L. and Davin, L.B. (2003) Crystal structures of pinoresinol-lariciresinol and phenylcoumaran benzylic ether reductases and their relationship to isoflavone reductases. J. Biol. Chem. 278, 50714–50723.
[12] Gang, D.R., Kasahara, H., Xia, Z.-Q., Vander Mijnsbrugge, K., Bauw, G., Boerjan, W., Van Montagu, M., Davin, L.B. and Lewis, N.G. (1999) Evolution of plant defense mechanisms relationships of phenylcoumaran benzylic ether reductases to pinoresinol-lariciresinol and isoflavone reductases. J. Biol. Chem. 274, 7516–7527.
[13] Ma, Q.-H. (2010) Functional analysis of a cinnamyl alcohol dehydrogenase involved in lignin biosynthesis in wheat. J. Exp. Bot. 61, 2735–2744.
[14] Kim, S.-J., Kim, M.-R., Bedgar, D.L., Moinuddin, S.G., Cardenas, C.L., Davin, L.B., Kang, C. and Lewis, N.G. (2004) Functional reclassification of the putative cinnamyl alcohol dehydrogenase multigene family in Arabidopsis. Proc. Natl. Acad. Sci. USA 101, 1455–1460.
[15] Mansell, D.J., Toogood, H., Waller, J., Hughes, J.M., Levy, C., Gardiner, J.M. and Scrutton, N.S. (2013) Biocatalytic asymmetric alkene reduction: crystal structure and characterization of a double bond reductase from Nicotiana tabacum. ACS Catal. 3, 370–379.
[16] Kasahara, H., Jiao, Y., Bedgar, D.L., Kim, S.-J., Patten, A.M., Xia, Z.-Q., Davin, L.B. and Lewis, N.G. (2006) *Pinus taeda* phenylpropenal double-bond reductase: Purification, cDNA cloning, heterologous expression in *Escherichia coli*, and subcellular localization in *P. taeda*. Phytochemistry 67, 1765–1780.
[17] Pereira, P.J.B., Macedo-Ribeiro, S., Párraga, A., Pérez-Luque, R., Cunningham, O., Darcy, K., Mantle, T.J. and Coll, M. (2001) Structure of human biliverdin IXβ reductase, an early fetal bilirubin IXβ producing enzyme. Nat. Struct. Mol. Biol. 8, 215–220.
[18] Cheng, A., Wang, L., Sun, Y. and Lou, H. (2013) Identification and expression analysis of key enzymes of the terpenoids biosynthesis pathway of a liverwort *Plagiochasma appendiculatum* by EST analysis. Acta. Physiol. Plant. 35, 107–118.

[19] Tamura, K., Dudley, J., Nei, M. and Kumar, S. (2007) MEGA4: molecular evolutionary genetics analysis (MEGA) software version 4.0. Mol. Biol. Evol. 24, 1596–1599.
[20] Trott, O. and Olson, A.J. (2010) AutoDock Vina: improving the speed and accuracy of docking with a new scoring function, efficient optimization, and multithreading. J. Comput. Chem. 31, 455–461.
[21] Koeduka, T., Watanabe, B., Suzuki, S., Hiratake, J., Mano, J.i and Yazaki, K. (2011) Characterization of raspberry ketone/zingerone synthase, catalyzing the alpha, beta-hydrogenation of phenylbutenones in raspberry fruits. Biochem. Biophys. Res. Co. 412, 104–108.
[22] Dick, R.A. and Kensler, T.W. (2004) The catalytic and kinetic mechanisms of NADPH-dependent alkenal/one oxidoreductase. J. Biol. Chem. 279, 17269–17277.
[23] Mano, J.I., Belles-Boix, E., Babiychuk, E., Inzé, D., Torii, Y., Hiraoka, E., Takimoto, K., Slooten, L., Asada, K. and Kushnir, S. (2005) Protection against photooxidative injury of tobacco leaves by 2-alkenal reductase. Detoxication of lipid peroxide-derived reactive carbonyls. Plant Physiol. 139, 1773–1783.